

MAC-DO: DRAM-Based Multi-Bit Analog In-Situ Accelerator for Matrix Multiplication Using Output Stationary Mapping

MINKI JEONG Wanyeong Jung
School of Electrical Engineering
KAIST

Abstract—Recently presented DRAM-based in-situ accelerators have shown their potentials in addressing the memory wall challenge of the traditional von Neumann architecture. Such accelerators exploit charge sharing or logic circuits for a simple logic operation at DRAM subarray level. However, their throughput is still limited because of low array utilization since only a few row cells in a DRAM array participate in the operations while most of rows in the array are deactivated. In addition, they require many cycles for more complex operations such as a multi-bit multiply-accumulate (MAC) operation, requiring a lot of overall data access and data movement, and it may worsen the power efficiency.

This paper presents MAC-DO, an efficient and low power DRAM-based in-situ accelerator, to address the above issues. Compared to previous DRAM-based in-situ accelerators, a MAC-DO cell (=two 1T1C DRAM cells) innately supports a multi-bit MAC operation for a single-cycle with good linearity and is still compatible with current 1T1C DRAM cell and array structure. This improvement is made possible by exploiting a new analog computation method based on charge steering. In addition, every MAC-DO cell in a DRAM array can simultaneously perform individual MAC operations without idle cells, leading to higher throughput and energy efficiency. Thus, a MAC-DO array can accelerate matrix multiplications based on output stationary mapping and thus supports most of the computations performed in deep neural networks (DNN). Our evaluation using transistor-level simulation shows that a test MAC-DO array with 16×16 MAC-DO cells achieves 120.96 TOPS/W and 97.07% Top-1 accuracy for MNIST dataset without retraining.

I. INTRODUCTION

Demand for processing a large amount of data efficiently keeps increasing in various areas such as edge devices [43], [45]. However, in a traditional computer architecture called von Neumann architecture, processing huge amount of data may be inefficient due to the high cost of data movement and a bottleneck between the cpu and memory [19], [54]. GPUs can mitigate the bottleneck problem since it performs parallel operations and reuses the data many times once it is read from the memory. However, it still has several limitations such as high cost and energy consumption [11].

Accelerator-in-memory (AiM) architecture can minimize the cost of data movement and avoid the memory bottleneck by performing computations within a memory [3], [6], [18], [20], [23], [50], [56]. One of the key design considerations of AiM architecture is how efficiently and effectively it can process a great amount of data parallelly under a restricted

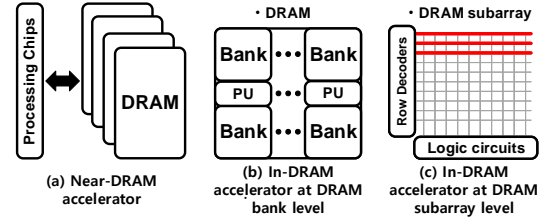


Fig. 1. Different types of DRAM-based accelerators

area around the memory. Accordingly, many different types of memory arrays such as SRAM and ReRAM have been actively investigated for AiM architectures [5], [32], [48], [49], [55], [57]. Even though SRAM based accelerators have been proved for its potential for computations [5], [14], [57], it still has a limitation of large cell area. ReRAM based accelerators also have superior computation ability, but may suffer from intrinsic data retention issues [7], [33]. Due to these limitations, data are usually stored in the main memory, which is DRAM in many systems, and a small portion of it is temporarily copied to these AiM arrays and processed. Even though the amount of data movement can be reduced by reusing the data inside the arrays, the overall performance of SRAM and ReRAM based AiMs is still limited by the long distance of data movement between the main memory and the AiM arrays.

On the other hand, DRAM-based AiMs can be placed close to the main memories of many computing systems and minimize the distance and amount of data movement between the processor and the main memory. Actually, many near-DRAM-based AiMs (Figure 1-(a)) have been developed and used in industry, including Google TPUs (HBM memories are used since TPUv2 [36]) and UPMEM PIM-DRAM [13]. Although the distance of data movement is shorter than SRAM and ReRAM based AiMs, most of the near-DRAM-based AiMs still require frequent data movement between individual DRAMs and data processing chips, which costs much more than on-chip data movement.

Monolithic integration of processing units (PU) and data storage in a single chip is one of the most power-efficient solutions. [9] used embedded DRAMs (eDRAMs) for such integration using a CMOS logic process technology, but the capacity of an eDRAM in a logic process is not as good

as a modern DRAM. Also, many in-DRAM data processing techniques and architectures have been presented recently. [4], [12], [24], [27]–[30], [42], [44], [46], [47]. In-DRAM accelerators are classified into two types depending on where data processing is performed within the DRAM hierarchy: at DRAM bank level or subarray level. [24], [27], [28], [47] place PUs close to DRAM banks (Figure 1-(b)) and process data efficiently through parallelism at bank level. However, their performance is still limited since they cannot exploit the full internal DRAM bandwidth because the bandwidth of each DRAM bank is designed to match that of device I/O. On the other hand, [4], [12], [29], [30], [42], [44], [46] can exploit the full internal DRAM bandwidth by processing data at subarray level. Such a so-called "DRAM-based in-situ accelerator" (Figure 1-(c)) no longer relies on common memory access operations for system memory, and can be altered for higher computational ability at the cost of more complicated array control.

However, previous DRAM-based in-situ accelerators have several challenges. They can perform only simple logic operations such as NOR and NOT for a computation cycle. For example, Ambit [44] uses *Triple Row Activation (TRA)* for a logic operation through charge sharing on BLs. DRISA [30] adds digital logic gates outside a DRAM array for a logic operation. DRISA's 3T1C modifies a 1T1C DRAM cell into a 3T1C DRAM cell for a logic operation. Thus, they still require a lot of overall data access and data movement for more complex operations such a multi-bit multiply-accumulate (MAC) operation. Even one multi-bit multiplication requires at least a few tens of cycles [29], and it may worsen the power efficiency for the MAC operation. Besides, they require additional data movement cost for copying the stored data into other rows or other DRAM arrays before a computation since DRAM read process is destructive. Above all, their throughput is still limited since only a few rows out of the entire DRAM array participate in operations while most of the cells are not activated for a computation cycle as shown in Figure 1-(c). It may be enough for accelerating some data-intensive tasks that memory bandwidth is a bottleneck, but it is not suitable for accelerating compute-intensive tasks, e.g. convolutions comprising over 90% computations and runtime of CNN operations [8], because of its low array utilization, throughput and power efficiency.

This paper presents MAC-DO, a high-performance DRAM-based in-situ accelerator, to efficiently perform MAC operations in a DRAM array. Figure 2 shows a proposed MAC-DO architecture and each block is detailed in Section III. In contrast with many previous DRAM-based in-situ accelerators, a MAC-DO cell, composed of two 1T1C cells in a DRAM array, supports a single-cycle MAC operation with multi-bit precision input and weight. For this, MAC-DO adopts a new analog computing mechanism based on charge steering, which was originally proposed for high-speed analog and mixed-signal circuits. It is basically a discrete-time analog amplifier with a voltage gain A_v between a V_{in} and a V_{out} , and its voltage gain is decided by the ratio of two capacitance values.

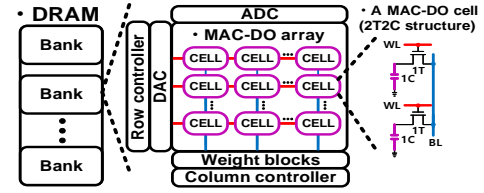


Fig. 2. Proposed MAC-DO architecture

Hence, the voltage gain is easily controllable by changing the size of one capacitor. This allows multiplication of two arbitrary numbers, regarding a differential analog signal V_{in} as an input multiplicand and the voltage gain A_v as the other.

In addition, MAC-DO is compatible with modern DRAM arrays and does not require any modifications of a DRAM cell and array for MAC operations. A MAC-DO cell requires only two 1T1C DRAM cells and all MAC-DO cells in a DRAM array can participate in parallel MAC computations at a time without an idle cell by employing an output stationary mapping [15], [34], [41]. Thus, a MAC-DO array can accelerate matrix multiplications for convolutions. It minimizes the overall data movement cost because each row and column of the MAC-DO cells shares same data, respectively, as many times as the array size once they are fetched from DRAM arrays. Thus, MAC-DO has much increased throughput and better energy efficiency than previous DRAM-based in-situ accelerators, even using a very small portion of banks and mats in a DRAM chip. Also, the overall integration cost of MAC-DO is expected to be low and can extend the range of AI applications to low-cost and low-power edge devices [53].

The main contributions of this paper are listed as follows:

- This paper presents a DRAM-based in-situ accelerator which implements charge-based analog MAC operations between multi-bit signed inputs and weights. It ensures higher linearity than current-based accelerators since capacitors are less susceptible to PVT variation [31], [51].
- A MAC-DO cell exploits charge steering technique that was originally used for analog and mixed-signal applications only. This paper first proves its applicability in highly parallel analog computing by proposing a 2-D array architecture, control methods, and error compensation schemes that are supported by extensive transistor-level simulation data. MAC-DO can take advantages of charge steering, including high-speed operation, good linearity and reliability, for analog computing as well.
- MAC-DO is compatible with modern DRAM array directly without any changes of DRAM cells. Hence, the overall integration cost of MAC-DO would be low.
- To the best of our knowledge, MAC-DO is the only architecture that can fully utilize the entire DRAM array for MAC operations. A MAC-DO cell performs a multi-bit MAC operation for a single cycle and every MAC-DO cell in a DRAM array participates in MAC operations simultaneously and each of them makes a different partial sum for MAC results. In addition, the data reusability is maximized in a MAC-DO array, minimizing data movement cost. As a result, MAC-DO can greatly improve

both the throughput and energy efficiency.

The rest of this paper is organized as follows. Section II introduces the background of DRAM and outer product for matrix multiplications. Section III describes charge-steering topology for MAC-DO, actual MAC-DO circuits and its operations. Section IV demonstrates digital and analog correction for negative weight and non-linear effects. Section V explains the evaluation methodology for performance test. Section VI presents the evaluation results of MAC-DO. Section VII concludes this paper.

II. BACKGROUND

A. DRAM and Its Operation

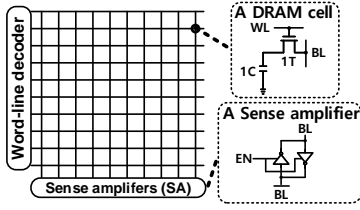


Fig. 3. DRAM MAT structure at subarray level

A DRAM chip consists of multiple banks connected by a global shared bus. Each bank is composed of subarray groups and each of them includes several cell matrices (mat), which is the basic unit of the DRAM chip. Each mat has its own independent sense amplifier (SA) row, a word-line (WL) decoder and a DRAM array. A SA amplifies the signal on a bit-line (BL) and quantizes it. A WL decoder controls WLs to write or read data. There are numerous DRAM cells inside a DRAM array and each cell consists of an access transistor and a cell capacitor, called a 1T1C cell as shown in Figure 3. The access transistors in a row are activated to write data into each cell or to read the data stored in each cell through WLs and BLs. For example, when writing data '1' into a cell, the corresponding WL is activated and its cell capacitor is charged to a high voltage through the corresponding BL. On the other hand, if the cell capacitor is discharged, the cell stores data '0'. In a read process, a row of access transistors is turned on and the stored data are read through the SAs.

B. Matrix Multiplications through Iterative Outer Products

A convolution layer (Figure 4) can be processed by repeating matrix multiplications [37], [52], and multiplication of two matrices A and B can be performed through iterative outer products between columns of A and rows of B [38]. First, each column of matrix A ($=I_k$) is multiplied by the corresponding row of matrix B ($=W_k$) as shown in Figure 5, forming a partial product ($=$ matrix O_k). Then, the partial products are added up, resulting in the product of A and B .

$$\sum_k O_i = \sum_k I_k \times W_k = [\sum_k A_{ik} \times B_{kj}] = A \times B \quad (1)$$

As this multiplication process involves a series of additions of partial product matrices with the same dimension, it can be easily mapped on a two-dimensional output-stationary MAC array. In each array cell, its horizontal input is multiplied by

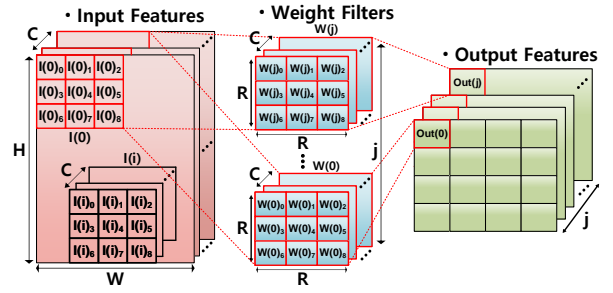


Fig. 4. Convolutions

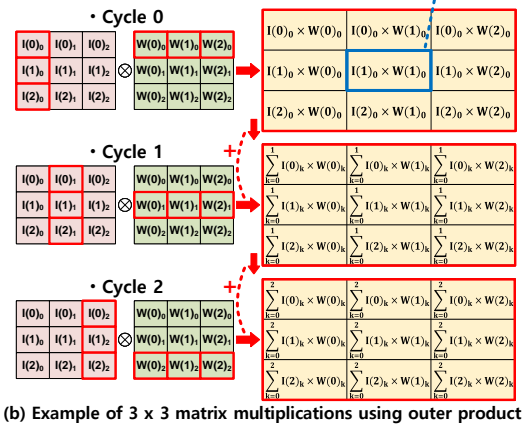
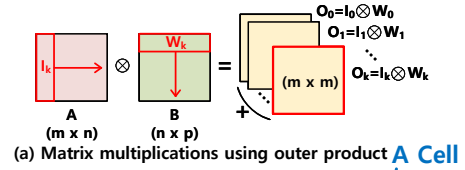


Fig. 5. Matrix multiplications through iterative outer products

the vertical input, and the result keeps accumulated in the same cell into an output matrix element ($=$ "Output Stationary"). Figure 5-(b) shows an example of matrix multiplication between two 3×3 matrices. Each cell performs individual MAC operations at each cycle and the final output matrix is formed after all cycles finish.

Section III-C explains how a MAC-DO cell operates as a MAC unit, and Section III-E shows how the MAC-DO cells can be combined into an output-stationary array that performs matrix multiplications for convolutions.

III. MAC-DO AND ITS OPERATION

A. Charge-Steering Amplifier

MAC-DO is based on a charge-steering topology [40]. Charge steering is originally for a discrete-time analog amplifier, offering high-speed and low-power amplification compared with traditional current-steering amplifiers. As far as we know, its application in high-performance analog computing is first proposed in this paper.

As shown in Figure 6, the charge-steering amplifier operates in two phases: reset phase and amplification phase. In the reset phase (Figure 6-(a)), two capacitors at the output terminals (C_D) are precharged to V_{DD} using two precharge ($PREC$) switches, while the tail capacitor C_T is reset to zero by turning

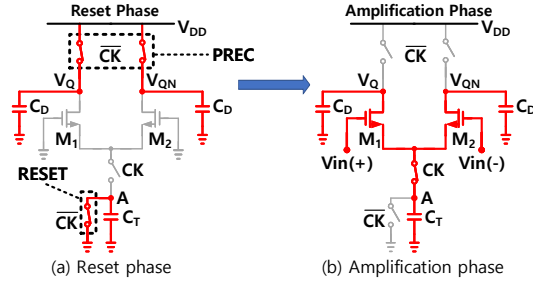


Fig. 6. The operation of a charge-steering amplifier

on the *RESET* switch. At the same time, the two transistors M_1 and M_2 are turned off in order to block charge flow between the capacitors. In the amplification phase (Figure 6-(b)), the *PREC* and *RESET* switches are turned off, and both transistors M_1 and M_2 are turned on with a differential input signal $V_{in} = V_{in(+)} - V_{in(-)}$. The tail capacitor C_T is connected to the differential pair M_1 and M_2 through a switch enabled by the clock signal CK . During the amplification phase, charges in output capacitors are discharged to the tail capacitor for a certain period, and the relative amount of discharge from two output capacitors are controlled by the differential input signal. Therefore, a differential voltage gain A_v is mainly determined by the ratio between the capacitance of C_T and C_D [40], with little dependence on the common mode voltage of V_{in} as

$$A_v \approx \frac{2C_T}{C_D}. \quad (2)$$

Hence, a differential output signal V_{out} is written as

$$V_{out} \approx V_{in} \times A_v. \quad (3)$$

where the V_{out} is the differential output voltage between the V_Q and V_{QN} . Consequently, multi-level V_{out} is generated as a product of two input variables: differential input voltage V_{in} and amplifier gain A_v (or C_T).

The charge-steering amplifier has two advantages over a traditional current-steering amplifier. First, its discrete operation is compatible with other digital circuits and helps save unnecessary power consumption. Secondly, it maintains stable operation even at high operating frequency up to a few GHz domains [10], [21]. These render the charge-steering topology also suitable for analog MAC operations where both the power efficiency and speed are required.

B. Mapping a Charge-Steering Amplifier onto Two 1T1C Cells

A DRAM array can be reorganized into an array of charge-steering amplifiers, or MAC-DO cells. Figure 7-(b) shows a modified charge-steering amplifier mapped on a DRAM array, which consists of two access transistors and two cell capacitors (two 1T1C DRAM cells). The tail node of the differential pair M_1 and M_2 in the charge-steering amplifier corresponds to the bit-line of the two 1T1C DRAM cells. Two *PREC* switches in the original charge-steering amplifier are combined with M_1 and M_2 with an extra *PREC* switch at the tail node, or the corresponding bit-line as shown in Figure 7-(b). In this modified charge-steering amplifier, V_Q and V_{QN} are

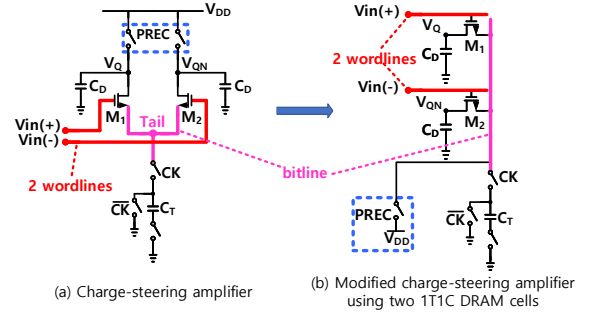


Fig. 7. A modified charge-steering amplifier by using two 1T1C DRAM cells

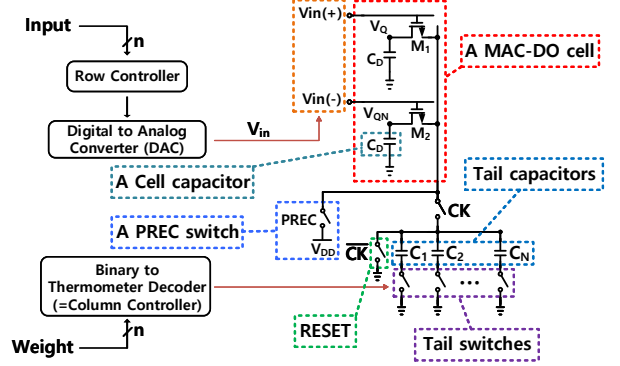


Fig. 8. A MAC-DO cell with peripheral circuits

precharged to V_{DD} by turning on M_1 , M_2 , and *PREC*. M_1 and M_2 transistors need to be turned on by a voltage higher than $V_{DD} + V_{TH}$ in order to fully precharge two DRAM cell capacitors to V_{DD} . During amplification, two WLs of the modified charge-steering amplifier receive $V_{in(+)}$ and $V_{in(-)}$ voltages composing a differential input V_{in} . Since Figure 7-(a) and Figure 7-(b) are identical except the position and the number of *PREC* switches, the modified charge-steering amplifier follows the same operation phases as discussed in Section III-A. As a result, a differential output signal V_{out} is generated from the two DRAM cells, at V_Q and V_{QN} .

C. A MAC-DO Cell for a Series of Multi-Bit MAC Operations

In order for the modified charge-steering amplifier to perform MAC operations with multi-bit input and weight data, V_{in} s and A_v s must be controllable by the input and weight data. It requires modifications on wordline and bitline drivers to the DRAM array MAC-DO cells are mapped on. In addition, a series of accumulations for an output stationary data flow involves a small change of operation phases.

1) *A MAC-DO cell and WL/BL drivers:* A MAC-DO cell consists of two DRAM cells as shown in Figure 8 and carries out multi-bit MAC operations within the cell. A multi-bit digital input is converted into a differential input signal V_{in} for M_1 and M_2 through a digital to analog converter (DAC). A multi-bit digital weight controls effective capacitance of the tail capacitor C_T by enabling a part of parallel tail capacitors through a thermometer code decoder, and therefore controls the gain of the amplifier, A_v . Here, a MAC-DO cell is located inside a DRAM array and the other circuits are in

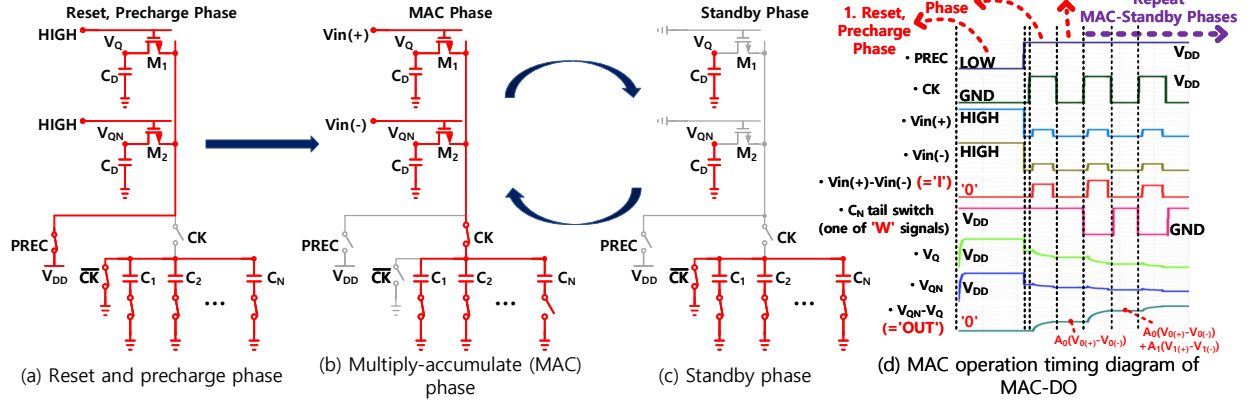


Fig. 9. MAC operation phase of MAC-DO

the array periphery. Each multiplication result is accumulated at the V_Q and V_{QN} as a differential signal V_{out} without additional precharge phases. This innate accumulation process necessitates an output stationary data flow for the array control since the MAC-DO cell is optimized for accumulating MAC outputs instead of storing input and weight data. The detailed MAC operation consists of three phases as follows.

2) *Phase 1. Reset and precharge phase:* In the first phase, a MAC-DO cell is prepared for following MAC operations as shown in Figure 9-(a). The $PREC$ switch, M_1 and M_2 are turned on, so that two cell capacitors are fully precharged to V_{DD} , resulting in $V_{out} = V_{QN} - V_Q = 0$. At the same time, the $RESET$ switch and all tail switches are turned on to reset all tail capacitors. These two operations are independent and both are carried out in this phase.

3) *Phase 2. Multiply-accumulate (MAC) phase:* In this phase, the $PREC$ and $RESET$ switches are turned off first. Then, a differential V_{in} signal corresponding to a multi-bit input is applied to M_1 and M_2 through a DAC. The A_v value is adjusted according to a multi-bit weight by controlling the tail switches through a thermometer code decoder. As a result, the MAC-DO cell performs multiplication of multi-bit input and weight and generates a differential output voltage V_{out} as

$$V_{out} = V_{in} \times \sum_{i=1}^N \frac{2C_i}{C_D} \quad (4)$$

, and the multiplication result V_{out} is accumulated at two cell capacitors as a differential voltage. Here, N determines the ratio of $\frac{C_i}{C_D}$ and hence the differential gain A_v . For example, if N is 2, two tail switches are turned on as shown in in Figure 9-(b) and it leads to $V_{out} = V_{in} \times \frac{2(C_1 + C_2)}{C_D}$. Higher N increases A_v and is used for greater weights. With a proper conversion between the analog and digital domains, the Equation (4) can be transformed as

$$OUT = I \times W \quad (5)$$

where OUT , I and W corresponds to V_{out} , V_{in} and $\sum_{i=1}^N \frac{2C_i}{C_D} = A_v$, respectively. Both the input (I) and weight (W) can be easily converted to corresponding analog values

(V_{in} and A_v) by using a DAC for V_{in} and a bank of tail capacitors for $A_v = \sum_{i=1}^N \frac{2C_i}{C_D}$.

4) *Phase 3. Standby phase:* After a MAC operation is performed in the MAC phase, M_1 and M_2 are turned off. Accordingly, the MAC result V_{out} is stored at two cell capacitors as a differential analog voltage (Figure 9-(c)). Meanwhile, all tail switches and the $RESET$ switch are turned on to reset all tail capacitors for the next MAC operation.

A final MAC result is obtained by repeating only the MAC phase and the standby phase alternately without additional precharge phases, retaining the previous MAC result at V_Q and V_{QN} . For instance, when next input and weight data are applied after the standby phase, the new multiplication is performed (Figure 9-(b)) and the new multiplication result is accumulated in the same capacitors (at V_Q and V_{QN}) with the previous MAC result. Output voltages stored in the cell capacitors barely affect the new multiplication because they are connected to the drains of the differential pair. Therefore, the final MAC result in the MAC-DO cell after a series of the MAC-standby phases can be expressed as

$$OUT_{FINAL} = \sum_i OUT_i = \sum_i I_i \times W_i \quad (6)$$

which is the same equation as a vector dot product operation, or a series of multiply-accumulate (MAC) operations.

Figure 9-(d) shows the detailed timing diagram for MAC operations of a MAC-DO cell. Since the MAC-DO cell performs a series of MAC operations without additional precharge phases once cell capacitors are precharged to V_{DD} in the beginning, it features an outstanding energy efficiency.

D. Array Structure

Multiple MAC-DO cells are combined and reorganized into an array for computing highly parallel MAC operations. A MAC-DO array is basically same as a DRAM array as shown in Figure 10. An input activation (I) is converted into a differential input voltage V_{in} and shared across a row of MAC-DO cells using two WLs. Similarly, a weight (W) controls a tail capacitor bank (=weight block) added to a bit-line and A_v , which is shared across a column through the bit-line.

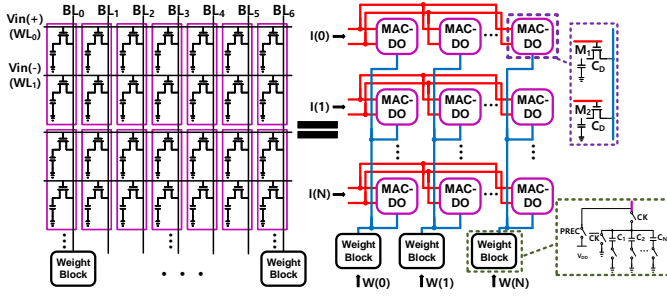


Fig. 10. A MAC-DO array structure

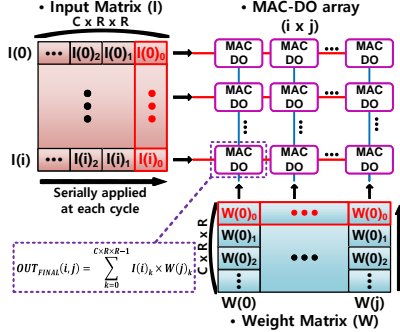


Fig. 11. Matrix multiplications in a MAC-DO array for convolutions

Thanks to these input and weight broadcasting, the MAC-DO array can calculate the outer product of two vectors (I and W) and accumulate the result in the array at every cycle. In this way, a MAC-DO array can efficiently calculate the product of two matrices. For input and weight matrices with proper sizes, every MAC-DO cell inside the array can be engaged in individual MAC operations without leaving an idle cell. Therefore, the MAC-DO array architecture has a high utilization ratio of up to 100% and high throughput compared to previous DRAM-based in-situ accelerators [4], [12], [29], [30], [42], [44], [46].

E. Matrix Multiplications using a MAC-DO array

Since each MAC result keeps accumulated in each MAC-DO cell, the MAC-DO array is controlled for an "output stationary" data flow [15], [34], [41]. To process a CNN layer using the MAC-DO array, $I(0) \sim I(i)$ and $W(0) \sim W(j)$ matrices in Figure 4 are reshaped as an input matrix (I) and a weight matrix (W) as shown in Figure 11. Then, the two matrices are multiplied through iterative outer products on the MAC-DO array. Each outer product is mapped on the MAC-DO array and keeps accumulated in each MAC-DO cell, resulting in an output activation

$$\sum OUT(i, j) = \sum_{k=0}^{C \times R \times R - 1} I(i)_k \times W(j)_k \quad (7)$$

where i and j mean the row and column number of the MAC-DO array, respectively, and k means the N 'th computation cycle. After the matrix multiplication is finished, every MAC-DO cell stores an individual MAC result simultaneously. With the matrix multiplications, MAC-DO can perform various convolution operations such as depth-wise convolution.

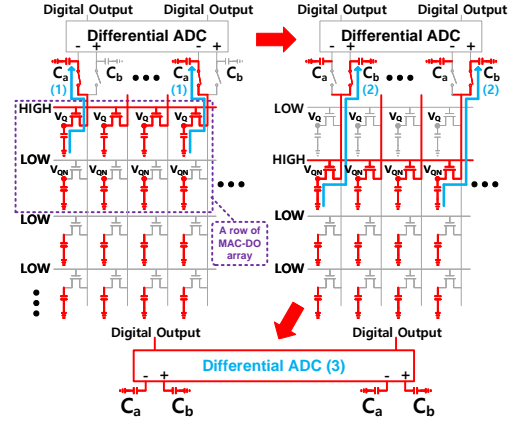


Fig. 12. ADC conversion of MAC results

The "output stationary" array control provides several benefits in terms of data movement. Once input and weight data are fetched from DRAM arrays, they are shared across each row and column of the MAC-DO array and reused as many times as the array size. Also, the MAC results are stationary within each MAC-DO cell for the entire matrix multiplication cycles. Thanks to this efficient data reuse for all three types of data, the MAC-DO array can efficiently minimize the data movement cost compared to previous in-situ accelerators [4], [12], [29], [30], [42], [44], [46].

F. Reading out MAC Results

Since each MAC-DO cell in a MAC-DO array stores an individual MAC result at its two cell capacitors as a differential analog voltage, MAC-DO requires an analog to digital converter (ADC) for reading out the stored result. A row of differential ADCs is connected to the MAC-DO array bitlines and quantizes the analog MAC results (Figure 12). Throughout the readout process, only a row of the MAC-DO array involves in the ADC conversion at a time while other rows are deactivated. One of two WLs of the row is activated first and analog voltages stored at V_Q nodes are sampled on a row of C_a capacitors and held (S/H). Next, the other WL is activated to sample the other part of differential voltages at V_{QN} on a row of C_b capacitors for a differential pair. Then, each ADC quantizes the differential analog voltage sampled on two capacitors (C_a and C_b). After a row of MAC results is read out, next rows go through the same readout process in a row-wise fashion.

G. Supporting Signed Number Operations

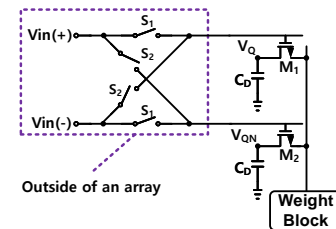


Fig. 13. Signed bit operations for input activation

1) *Signed input*: Because an input activation is translated into a differential analog voltage, MAC-DO easily supports negative activation by flipping its polarity. This requires only a few additional switches as shown in Figure 13. The circuit is unchanged when S_1 switches are on. On the other hand, when S_2 s are on, the polarity of the differential input signal V_{in} is inverted inside the corresponding MAC-DO cells and a multiplication with negative input

$$OUT = -I \times W \quad (8)$$

occurs in the MAC-DO cells. This adds an extra sign bit for input and increases the bit precision.

2) *Signed weight*: The charge-steering circuit always discharges from the DRAM cell capacitors, so a MAC-DO cell itself cannot handle negative or zero weight data. Also, because of the innate tail capacitance offset arising from parasitic capacitors at the BL and capacitor bank, the weight term (W) in Equation (5) is biased and needs correction. In order to resolve both issues, a digital offset is added to weights before going into the array. So, the Equation (6) for MAC operation is modified as

$$\begin{aligned} \sum OUT &= \sum I \times (W + W_o + 2^{N-1}) \\ &= \sum I \times (W + W_c) \end{aligned} \quad (9)$$

where W_o is the offset from parasitic capacitors, N is the weight bit-precision including a signed bit and 2^{N-1} is a digitally added value for shifting negative weights into positives.

IV. MISMATCH CORRECTION METHODS

A. Mismatch Effect of MAC-DO Cells

Since every access transistor in a MAC-DO array performs analog MAC operations, the mismatch among the access transistors affects MAC operations in a real chip. As a result, outputs generated in two MAC-DO cells can be different even with the same input and weight data. In order to minimize such mismatch effects in MAC operations, three methods are used in MAC-DO circuit design and operation. First, the size of cell transistors are increased to reduce the mismatch. Even though this has largely increased the power consumption for driving cell transistors, it still maintains good energy efficiency. Secondly, the mismatch effect is further diminished by adopting a common centroid layout technique. For the common centroid layout, each MAC-DO cell is copied and placed symmetrically about both axes of symmetry x and y as shown in Figure 14. All the copied cells can be placed in a DRAM array without altering the original DRAM array structure. These copied cells are activated at the same time with the same data. For example, 4 cells of 'E' in Figure 14 are placed symmetrically inside a DRAM array and operate simultaneously. This technique may reduce the effect of spatial mismatch gradient with less cell area increase.

Despite those two solutions for reducing the mismatch effect, it is not fully removed in reality. With the mismatch effect, the Equation (9) is expressed as

$$\sum OUT = \sum (I + I_m) \times (W + W_c) \quad (10)$$

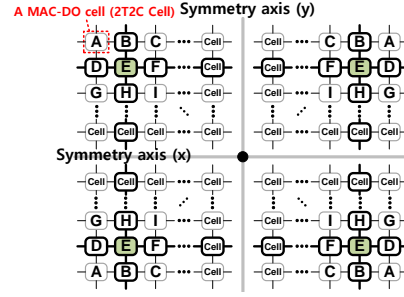


Fig. 14. Common centroid layout for reducing mismatch effect

where I_m represents the offset mismatch of each MAC-DO cell. Thus, MAC-DO requires additional correction techniques to cancel the offset terms (I_m and W_c) to acquire an actual MAC result, which is expressed as $\sum I \times W$.

B. Digital Correction

To get the desired MAC result $\sum I \times W$, the left and right sides of Equation (10) are transposed as

$$\sum I \times W = \sum OUT - I_m \sum W - W_c \sum I - \sum I_m W_c \quad (11)$$

, so the offset effects included in $\sum OUT$ need to be subtracted to get the desired MAC result. The offset constants of I_m and W_c are obtained by applying the test data composed of '1' and '0' and by solving the equation above. For this correction, MAC-DO needs additional accumulations of input and weight data in digital domain, but its overhead is not critical in the entire system, since the offset constants can be reused once they are obtained and other accumulation results can also be shared across many cells in a row or column.

C. Analog Correction

In addition to the digital correction, MAC-DO can use an analog offset cancellation technique such as chopping. For this, MAC-DO performs an additional MAC operation with negated input and weight after a normal MAC cycle. The two MAC operation results, OUT and OUT' , are

$$\begin{aligned} OUT &= (I + I_m) \times (W + W_c) \\ OUT' &= (-I + I_m) \times (-W + W_c), \end{aligned} \quad (12)$$

and they add up to

$$OUT + OUT' = 2(I \times W + I_m \times W_c). \quad (13)$$

Therefore, the desired MAC result is expressed as

$$\sum I \times W = (\sum OUT + OUT' - \sum I_m W_c) / 2 \quad (14)$$

Now the MAC result has only one constant subtraction term that can be easily found and computed; It no longer requires accumulation of input nor weight data.

V. EVALUATION METHODOLOGY

A. Overall System Architecture for Testing MAC-DO

To verify the performance of MAC-DO, an overall system architecture including test circuits has been designed as shown in Figure 15. The test focuses on accelerating compute-intensive convolutions in inference which are the largest

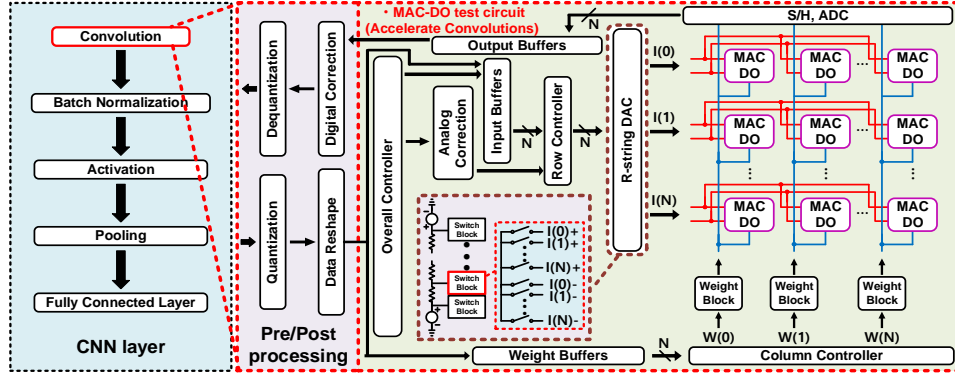


Fig. 15. Overall system architecture for testing MAC-DO

bottleneck in CNN layers ($> 90\%$ computations, runtime). The MAC-DO for accelerating convolutions mainly consists of five blocks: a MAC-DO array, a row controller, an R-string DAC block, a column controller, and an analog to digital converter (ADC) block.

For convolutions, input and weight data are stored outside of MAC-DO, which would be DRAM arrays. Those data are quantized and go through a data-reshaping step to be prepared as a matrix form to perform matrix multiplications like Figure 11. Then, the row controller receives the input matrix through input buffers and controls the R-string DAC to generate differential analog input voltages for corresponding rows of MAC-DO cells. The column controller receives the weight matrix through weight buffers and manipulates the tail switches of the capacitor banks in weight blocks. After a series of MAC operations inside the array, the ADCs convert the differential analog output voltages stored at each MAC-DO cell into digital values row by row. Then, digital correction is performed and the digital values are dequantized. Data pre/post processing and running other layers such as pooling and activation are performed with the help of software using the host CPU because they are rather data-intensive and can be easily performed using conventional in-/near-DRAM processing techniques. Detailed software/system support is out of the scope of this paper and planned as future work.

B. Parameters of MAC-DO Test Circuits

TABLE I
DESIGN PARAMETERS OF MAC-DO TEST CIRCUIT

Technology	65nm CMOS logic process
Supply voltage (V_{DD})	1.2V
Clock frequency	12.5 (MHz)
An access transistor size (W/L)	800/560 (nm)
Cell capacitance	100f (F)
Noise at cell capacitors	264.3 μ V, $< 0.13\%$ error
Each tail capacitance	6.8f~9.6f (F)
A MAC-DO cell size	221.21 (μm^2)
An array size	16 \times 16
Input/weight precision	4bit/4bit integer
# of maximum MAC operations in a MAC-DO cell	200 (10.6 fJ/MAC)

Major design parameters of the test circuit are shown in Table I. The circuit has been designed using 65nm CMOS

logic process and is powered by 1.2V supply voltage. Though the circuit can operate much faster, the clock frequency is set relatively slower to verify the robustness of the MAC-DO cell in one of the worse cases, as unwanted effects of leakage currents increase with longer period. The size of access transistors is selected larger than a usual 65 nm design to reflect the methods for reducing mismatch effects ($> 10 \times 4$, 10 larger transistor size than normal design and 4 from common centroid). The MAC-DO array size is set as 16×16 for only the test, and hence cell capacitance is chosen relatively larger than normal DRAM cell capacitance to adjust A_v . The cell capacitance can be scaled down at realistic DRAM array size. Since one MAC result of a MAC-DO cell is over 200 mV after 150 MAC operations, the error of output noise is less than 0.13% out of the final MAC result. Each tail capacitor is sized to perform MAC operations with minimum linearity errors. The test circuit is optimized to target 4b \times 4b of input and weight data precision, but it can be flexibly changed depending on the target noise levels and area for weight blocks in the array periphery. With these circuit parameters, a MAC-DO cell can perform a series of up to 200 MAC operations without precharging the output capacitors again. This can be further increased depending on the clock frequency, tail capacitance and levels of wordline input voltages V_{in} .

C. Circuit Implementation

MAC-DO has been simulated in transistor level by using Cadence Spectre Simulator [1] under a 65nm CMOS process. The MAC-DO array (16 \times 16 MAC-DO cells or 32 \times 16 1T1C DRAM cells), row controller (including switch blocks), R-string DAC and column controller have been designed in transistor level. For ADC analysis, we use data from a survey of recent ADC circuits [35] and scaled an ADC data to 65nm process, 1.2V supply voltage and 6bit output precision. We assume 16 ADCs (= # of columns) are used and each ADC area is 0.00116mm² with 0.89 (pJ) per 6bit conversions. The test focuses on accelerating convolutions of a neural network. The 4bit quantized input and weight data at each convolution layer are extracted through PyTorch [39] and they are transferred into the Spectre simulator by using a Verilog-A

block modeling a data bus [16]. After a simulation is finished, differential analog output voltages of the simulated array are directly observed from every MAC-DO cell at the same time and delivered to PyTorch to dequantize the analog MAC results and run remaining layers.

D. Dataset and Network for Benchmarking

TABLE II
LENET-5 NEURAL NETWORK FOR CIRCUIT SIMULATION

Dataset	MNIST [25]
Network	LeNet-5 [26]
Batch size	32
Layers	Network Parameters
Conv1(C1)	Input Feature : 1 x 32 x 32
BatchNorm, Tanh	Weight Filter : 6 x 1 x 5 x 5
Conv3(C3)	Input Feature : 6 x 14 x 14
BatchNorm, Tanh	Weight Filter : 16 x 6 x 5 x 5
Conv5(C5)	Input Feature : 16 x 5 x 5
BatchNorm, Tanh	Weight Filter : 120 x 16 x 5 x 5
FC1	Input Feature : 120 x 1
Tanh	Weight Filter : 84 x 120
FC2	Input Feature : 84 x 1
	Weight Filter : 10 x 84

TABLE III
BENCHMARKING TOP-1 ACCURACY FOR MNIST DATASET IN LEnet-5

I/W precision	full-precision	4b/4b	3b/3b	2b/2b
Top-1 Accuracy	99.075%	98.973%	98.595%	84.767%

To verify general matrix to matrix multiplication (GEMM) on the MAC-DO array, MAC-DO's computation accuracy has been tested in the same way as [22] by measuring the Top-1 accuracy drops when MAC-DO performs MAC operations for a convolution layer of LeNet-5 [26] neural network for MNIST dataset [25]. Other layers such as non-linear function have been supported by using software. The detailed network parameters of LeNet-5 is shown in Table II. In order for benchmarking, the LeNet-5 network for MNIST dataset is pre-trained with full precision operations and batch size 32 using PyTorch, and the Top-1 accuracy shows 99.075%. Also, a convolution layer in LeNet-5 has been digitally computed after 4bit, 3bit and 2bit quantization to compare with analog computation using MAC-DO. For these tests, the pre-trained network in full precision domain has been reused without retraining and a digital correction is performed using PyTorch. The accuracy for the each case is shown in Table III.

VI. EVALUATION RESULTS

A. Accuracy of Multiplication Results of A MAC-DO Cell

TABLE IV
EFFECTS OF DIGITAL AND ANALOG MISMATCH CORRECTION METHODS

Correction	No correction	Digital	Digital+Analog
Error range(%)	~4.06%	~2%	~0.23%

Figure 16 shows the accuracy of multiplication results of a MAC-DO cell. Figure 16-(a) shows the accuracy of repetitive MAC operations in a MAC-DO cell. For example, the plot with square markers shows the accumulation results (V_{out}) of a series of $15(I) \times 15(W)$ multiplications. Results with $W = 0$, show that non-zero multiplication results keep accumulating

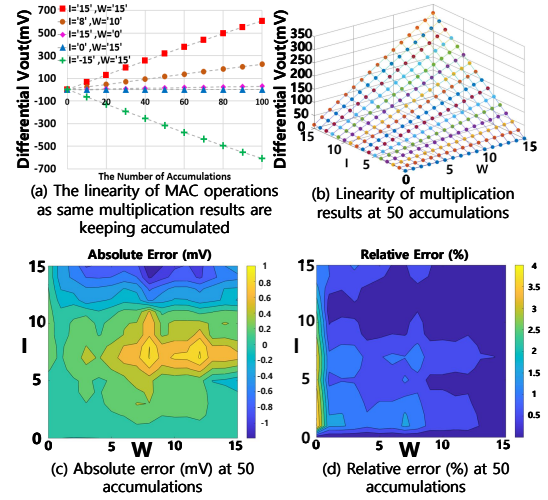


Fig. 16. The linearity of multiplication results of a MAC-DO cell and its errors

because of the weight offset arising from parasitic capacitors in weight blocks. However, this unwanted offset can be removed by aforementioned correction techniques. Figure 16-(b) shows the multiplication results for all 256($4b \times 4b$) combinations of inputs and weights, after 50 times of accumulation in a MAC-DO cell. Figure 16-(c) and (d) shows the absolute (mV) and relative errors (%) of the data in Figure 16-(b) from the ideal values. The maximum error levels among the 256 results are 1.19mV and 4.06%, respectively. Table IV shows the relative error after digital and analog correction with mismatch effects. Analog correction requires doubled MAC cycles but shows much better correction performance.

B. Inference Accuracy of MAC-DO

The inference accuracy of MAC-DO analog computation results has been tested with C3 layer of LeNet-5. For the test, C3 convolution layer is executed by the MAC-DO test circuit using transistor-level simulation for 448 test set images from the MNIST dataset, and the Top-1 accuracy is calculated from the collection of the final results. Other layers have been executed with full precision using software in the similar way as [22]. In order to dequantize the analog MAC results, we use four images as training data to find proper dequantization parameters. The Top-1 accuracy is 97.07% with a standard deviation of 0.2507%, (without network retraining, the four images for training dequantization parameters are not included). To estimate an effective bit precision of this analog computing, the Top-1 accuracy is compared to the accuracy results when the same C3 layer only has been executed after quantization into 2-, 3-, 4-bit data (Table III). The Top-1 accuracy drop of 1.903% from the MAC-DO analog computing is most similar to that of digital operation with 3-bit quantized data. The accuracy number can be further improved by retraining the LeNet-5 network with MAC-DO circuits or performing additional analog corrections.

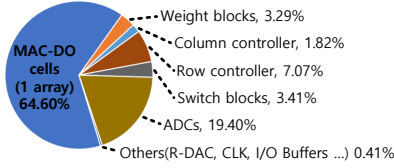


Fig. 17. Area breakdown of MAC-DO architecture

C. Area Estimation of the Test Circuit

The area of each block in the MAC-DO test circuit has been estimated based on the transistor-level circuit design and layout. The total area is estimated 0.096mm² and Figure 17 shows the area breakdown. Currently, most of the area is for the 16×16 array (64.6%), mainly due to large areas for cell capacitors since capacitors are designed horizontally in CMOS logic technology. The area for the ADCs makes up 19.40% of the total area. The ADC overheads can be minimized by sharing one ADC with multiple BLs through multiplexers at the expense of longer readout latency. The area for the weight blocks accounts for 3.29% of the total area, which is also dominated by the tail capacitors. The area of switch blocks accounts for 3.41% and the area of row controller is 7.07% of the total area because of a lot of switches in row periphery. The overall area of the MAC-DO architecture can be further decreased by using DRAM technology because DRAM cell capacitors are designed vertically. In addition, the size of an access transistor can be scaled down to an actual access transistor size in DRAM. Given common centroid layout, the mismatch effect can be further minimized as more cells are activated at the same time. So, minimizing mismatch is boiled down to selecting how many cells regardless of cell size, but it would lower the throughput. Also, the switch transistors in the row controller can be much smaller by using normally sized access transistors ($\sim 10\times$ smaller even with common centroid cell mapping) in the array because smaller access transistors require less driving force for the switches.

D. Average Power Breakdown

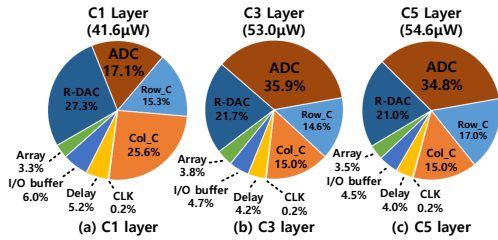


Fig. 18. Average power breakdown of three convolution layers (C1, C3 and C5)

Figure 18 shows the average power breakdown of the MAC-DO test circuit for running three convolution layers C1, C3 and C5 of LeNet-5. The total power for C1, C3 and C5 layers are 41.6 μW, 53.0 μW and 54.6 μW, respectively. The power consumption for precharging cell capacitors is dominant in the array power because MAC operations in MAC-DO are performed by discharging cell capacitors that were precharged once at the precharge phase. The array power consumption in

the C1 layer is smaller than in the C3 and C5 layers because it requires the fewest accumulation cycles for a convolution ($5\times 5 = 25$ cycles). The ADCs account for large portion of the total power. The R-DAC also shows significant power consumption in the MAC-DO test circuit because it drives a lot of big access transistors ($\sim 40\times$ bigger than usual), so it can be further reduced by optimizing the size of access transistors in DRAM process. In addition, since the size of a cell capacitor is smaller in actual DRAM process, the size of tail capacitors can also be scaled down, and so does the power consumption of the column controller (Col_C) and the MAC array in a real DRAM based chip.

E. Performance Analysis and Comparison

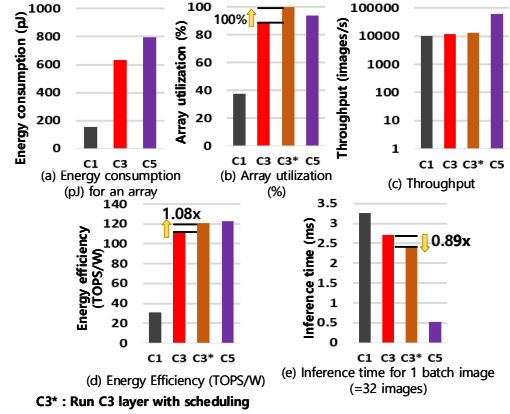


Fig. 19. Performance comparison among convolution layers

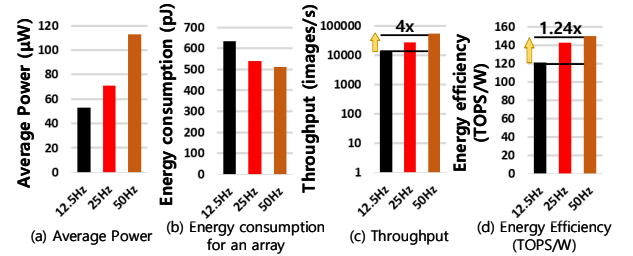


Fig. 20. Performance comparison at faster speeds

Figure 19 summarizes the performance numbers from the circuit simulation results of the MAC-DO test circuit on three convolution layers (C1, C3, C5) of LeNet-5. Figure 19-(a) shows the total energy consumption for executing an array operation (a part of convolution that fits in the 16 x 16 array). Figure 19-(b) shows the average array utilization (used MAC-DO cells / total MAC-DO cells) for each convolution layer, which marks high ($\sim 93.75\%$) utilization except for the C1 layer with unusually few numbers of input and output channels (1 and 6, respectively). Figure 19-(c) shows the throughput in terms of images per second. Figure 19-(d) shows the energy efficiency (TOPS/W), where 1 MAC operation is regarded as 2 operations (1 multiply + 1 accumulate). Since C1 has the lowest array utilization, its energy efficiency is the lowest among the three layers. Figure 19-(e) shows inference time for a batch of images (=32 images). If a part of image data can be processed with the next image using scheduling, the

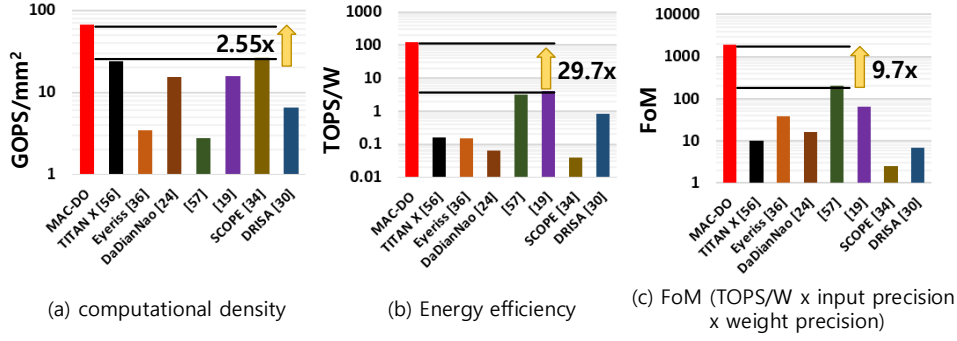


Fig. 21. Performance comparison with other works

TABLE V
BASELINE DESCRIPTIONS FOR OTHER WORKS

	GPU	Digital Accelerator		SRAM-Based CiM		DRAM-Based In-Situ Accelerator		
	TITAN-X [2] ¹	Eyeriss [8]	DaDianNao [9] ²	[17]	[14] ²	SCOPE [29]	DRISA [30] ³	MAC-DO
Tech	28nm	65nm	28nm	65nm	7nm	22nm	22nm	65nm
I/W Precision	INT8	16b fixedpoint	INT16,32	8b/8b	4b/4b	logic operation	logic operation	4b/4b
Throughput	40.4 TOPS	42 GOPS	5.58 TOPS	4 GOPS	372.4 GOPS	7.2 TOPS	1.68 TOPS	6.4 GOPS
Workload		CNN	CNN	SVM	CNN	CNN, RNN	CNN	CNN

¹ Normalized to INT8, ² Scaled to 65nm, assume energy and area \propto Tech², ³ re-evaluated to 8Gb capacity

TABLE VI
PERFORMANCE ESTIMATION AT REALISTIC ARRAY SIZE

Power	Throughput	Energy efficiency
17.46 (mW)	3.26 TOPS (509.4 \times)	186.7 TOPS/W (1.54 \times)

array utilization can increase to 100% for C3 layer, because the number of its output channels (=16) is a multiple of the number of columns (=16) in the MAC-DO array. In this case (=C3*), the energy efficiency and inference time for a batch of images show 1.08 \times and 0.89 \times improvement over when without scheduling, respectively.

Figure 20 shows the performance summary for faster clock frequency settings. The throughput increases linearly to clock frequency because the time for precharging cell capacitors does not affect precharging numbers due to the small array size. Also, it shows better energy efficiency at faster speeds as excessive energy dissipation during too long evaluation periods is reduced, even though the average power is increased.

F. Performance Estimation for a Real DRAM Based Array

In this section, we estimate MAC-DO architecture's performance when it is used with a real DRAM array size. The array size is scaled to a typical DRAM MAT size (256 \times 512 MAC-DO cells, or 512 \times 512 1T1C DRAM cells [58]). Our estimation is based on the average power breakdown of C3 layer (Figure 18-(b)) and the size of cell capacitors and access transistors are unchanged. Then, we assume the average power is linear to the number of circuit blocks because most power dissipation is due to the dynamic power consumption, which is basically proportional to the size of parasitic capacitors. Overheads for controlling complicated row and column peripheral circuits are amortized over more number of MAC-DO cells, so the estimated performance of MAC-DO marks 1.54 \times energy efficiency improvement over the 16 \times 16 test circuit (Table

VI) with 3.26 TOPS of throughput over when the array size is 16 \times 16.

G. Comparison with Other Works

Figure 21 compares the results with DRAM-based in-situ accelerators that perform CNN operations, a common GPU and other accelerators [2], [8], [9], [14], [17], [29], [30], and Table V shows their baseline descriptions for the comparison. Since MAC-DO array size is 16 \times 16, the test chip has a low throughput, but in a real chip, it can be easily scaled to several TOPS as shown in Table VI. Figure 21-(a) compares computational density (GOPS/mm²) with other works. MAC-DO shows 2.55 \times computational density improvement over a recent DRAM-based in-situ accelerator [29] thanks to high array utilization. In addition, the computational density will be further increased when MAC-DO is designed using DRAM technology. Figure 21-(b) shows that MAC-DO is at least minimum 29.7 \times more energy efficient than other compared works. Figure 21-(c) compares the FoM (energy efficiency(TOPS/W) \times input precision \times weight precision), and MAC-DO also marks the best with > 9.7 \times difference with previous works.

VII. CONCLUSION

Recently presented DRAM-based in-situ accelerators can perform only simple logic operations because an efficient way to accelerate MAC operations suitable to DRAM technology has not been presented so far. Also, the energy efficiency and throughput of those previous works are limited because of low array utilization. To resolve this issue, MAC-DO performs analog multi-bit precision multiply-accumulate operations directly using the 1T1C DRAM array and can achieve 100% array utilization by exploiting a very compact, charge-steering based analog multiplication mechanism. MAC-DO's core MAC operation happens inside each 2T2C MAC-DO cell

and does not involve complex digital circuits so it is well suited to DRAM technologies. The output stationary data flow allows easy task mapping on the MAC-DO array and efficient data reuse for all types of data, leading to the improvement of throughput and energy efficiency for most convolution layers. Thanks to the high array utilization, MAC-DO shows $> 2.55\times$ higher computational density than previous DRAM-based in-situ accelerators and $> 29.7\times$ energy efficiency and $> 9.7\times$ over all compared accelerators.

REFERENCES

- [1] "cadence spectre circuit simulator." www.cadence.com.
- [2] "Nvidia gpu." <http://www.nvidia.com>, 2016.
- [3] J. Ahn, S. Hong, S. Yoo, O. Mutlu, and K. Choi, "A scalable processing-in-memory accelerator for parallel graph processing," in *Proceedings of the 42nd Annual International Symposium on Computer Architecture*, 2015, pp. 105–117.
- [4] S. Angizi and D. Fan, "Redram: A reconfigurable processing-in-dram platform for accelerating bulk bit-wise operations," in *2019 IEEE/ACM International Conference on Computer-Aided Design (ICCAD)*. IEEE, 2019, pp. 1–8.
- [5] A. Biswas and A. P. Chandrakasan, "Conv-ram: An energy-efficient sram with embedded convolution computation for low-power cnn-based machine learning applications," in *2018 IEEE International Solid-State Circuits Conference (ISSCC)*. IEEE, 2018, pp. 488–490.
- [6] M. N. Bojnordi and E. Ipek, "Memristive boltzmann machine: A hardware accelerator for combinatorial optimization and deep learning," in *2016 IEEE International Symposium on High Performance Computer Architecture (HPCA)*. IEEE, 2016, pp. 1–13.
- [7] Y. Chen, "Reram: History, status, and future," *IEEE Transactions on Electron Devices*, vol. 67, no. 4, pp. 1420–1433, 2020.
- [8] Y.-H. Chen, J. Emer, and V. Sze, "Eyeriss: A spatial architecture for energy-efficient dataflow for convolutional neural networks," *ACM SIGARCH Computer Architecture News*, vol. 44, no. 3, pp. 367–379, 2016.
- [9] Y. Chen, T. Luo, S. Liu, S. Zhang, L. He, J. Wang, L. Li, T. Chen, Z. Xu, N. Sun *et al.*, "Dadiannao: A machine-learning supercomputer," in *2014 47th Annual IEEE/ACM International Symposium on Microarchitecture*. IEEE, 2014, pp. 609–622.
- [10] S.-H. W. Chiang, H. Sun, and B. Razavi, "A 10-bit 800-mhz 19-mw cmos adc," *IEEE Journal of Solid-State Circuits*, vol. 49, no. 4, pp. 935–949, 2014.
- [11] S. Collange, D. Defour, and A. Tisserand, "Power consumption of gpus from a software perspective," in *International Conference on Computational Science*. Springer, 2009, pp. 914–923.
- [12] Q. Deng, L. Jiang, Y. Zhang, M. Zhang, and J. Yang, "Dracc: a dram based accelerator for accurate cnn inference," in *Proceedings of the 55th Annual Design Automation Conference*, 2018, pp. 1–6.
- [13] F. Devaux, "The true processing in memory accelerator," in *2019 IEEE Hot Chips 31 Symposium (HCS)*, 2019, pp. 1–24.
- [14] Q. Dong, M. E. Sinangil, B. Erbagci, D. Sun, W.-S. Khwa, H.-J. Liao, Y. Wang, and J. Chang, "15.3 a 351tops/w and 372.4 gops compute-in-memory sram macro in 7nm finfet cmos for machine-learning applications," in *2020 IEEE International Solid-State Circuits Conference (ISSCC)*. IEEE, 2020, pp. 242–244.
- [15] Z. Du, R. Fasthuber, T. Chen, P. lenne, L. Li, T. Luo, X. Feng, Y. Chen, and O. Temam, "Shidiannao: Shifting vision processing closer to the sensor," in *Proceedings of the 42nd Annual International Symposium on Computer Architecture*, 2015, pp. 92–104.
- [16] D. FitzPatrick and I. Miller, *Analog behavioral modeling with the Verilog-A language*. Springer Science & Business Media, 1998.
- [17] S. K. Gonugondla, M. Kang, and N. Shanbhag, "A 42pj/decision 3.12 tops/w robust in-memory machine learning classifier with on-chip training," in *2018 IEEE International Solid-State Circuits Conference (ISSCC)*. IEEE, 2018, pp. 490–492.
- [18] P. Gu, X. Xie, Y. Ding, G. Chen, W. Zhang, D. Niu, and Y. Xie, "ipim: Programmable in-memory image processing accelerator using near-bank architecture," in *2020 ACM/IEEE 47th Annual International Symposium on Computer Architecture (ISCA)*. IEEE, 2020, pp. 804–817.
- [19] S. Han, X. Liu, H. Mao, J. Pu, A. Pedram, M. A. Horowitz, and W. J. Dally, "Eie: Efficient inference engine on compressed deep neural network," *ACM SIGARCH Computer Architecture News*, vol. 44, no. 3, pp. 243–254, 2016.
- [20] M. Imani, S. Gupta, Y. Kim, and T. Rosing, "Floatpim: In-memory acceleration of deep neural network training with high precision," in *2019 ACM/IEEE 46th Annual International Symposium on Computer Architecture (ISCA)*. IEEE, 2019, pp. 802–815.
- [21] J. W. Jung and B. Razavi, "A 25-gb/s 5-mw cmos cdr/deserializer," *IEEE Journal of Solid-State Circuits*, vol. 48, no. 3, pp. 684–697, 2013.
- [22] S. Jung, H. Lee, S. Myung, H. Kim, S. K. Yoon, S.-W. Kwon, Y. Ju, M. Kim, W. Yi, S. Han *et al.*, "A crossbar array of magnetoresistive memory devices for in-memory computing," *Nature*, vol. 601, no. 7892, pp. 211–216, 2022.
- [23] Y. Kim, M. Imani, and T. S. Rosing, "Image recognition accelerator design using in-memory processing," *IEEE Micro*, vol. 39, no. 1, pp. 17–23, 2018.
- [24] Y.-C. Kwon, S. H. Lee, J. Lee, S.-H. Kwon, J. M. Ryu, J.-P. Son, O. Seongil, H.-S. Yu, H. Lee, S. Y. Kim, Y. Cho, J. G. Kim, J. Choi, H.-S. Shin, J. Kim, B. Phuah, H. Kim, M. J. Song, A. Choi, D. Kim, S. Kim, E.-B. Kim, D. Wang, S. Kang, Y. Ro, S. Seo, J. Song, J. Youn, K. Sohn, and N. S. Kim, "25.4 a 20nm 6gb function-in-memory dram, based on hbm2 with a 1.2tflops programmable computing unit using bank-level parallelism, for machine learning applications," in *2021 IEEE International Solid-State Circuits Conference (ISSCC)*, vol. 64, 2021, pp. 350–352.
- [25] Y. LeCun, C. Cortes, and C. Burges, "The mnist database of handwritten digits." <http://yann.lecun.com/exdb/mnist/>.
- [26] Y. LeCun, L. Bottou, Y. Bengio, and P. Haffner, "Gradient-based learning applied to document recognition," *Proceedings of the IEEE*, vol. 86, no. 11, pp. 2278–2324, 1998.
- [27] S. Lee, K. Kim, S. Oh, J. Park, G. Hong, D. Ka, K. Hwang, J. Park, K. Kang, J. Kim *et al.*, "A lynn 1.25 v 8gb, 16gb/s/pin gddr6-based accelerator-in-memory supporting 1tflops mac operation and various activation functions for deep-learning applications," in *2022 IEEE International Solid-State Circuits Conference (ISSCC)*, vol. 65. IEEE, 2022, pp. 1–3.
- [28] S. Lee, S.-h. Kang, J. Lee, H. Kim, E. Lee, S. Seo, H. Yoon, S. Lee, K. Lim, H. Shin *et al.*, "Hardware architecture and software stack for pim based on commercial dram technology: Industrial product," in *2021 ACM/IEEE 48th Annual International Symposium on Computer Architecture (ISCA)*. IEEE, 2021, pp. 43–56.
- [29] S. Li, A. O. Glova, X. Hu, P. Gu, D. Niu, K. T. Malladi, H. Zheng, B. Brennan, and Y. Xie, "Scope: A stochastic computing engine for dram-based in-situ accelerator," in *2018 51st Annual IEEE/ACM International Symposium on Microarchitecture (MICRO)*. IEEE, 2018, pp. 696–709.
- [30] S. Li, D. Niu, K. T. Malladi, H. Zheng, B. Brennan, and Y. Xie, "Drissa: A dram-based reconfigurable in-situ accelerator," in *2017 50th Annual IEEE/ACM International Symposium on Microarchitecture (MICRO)*. IEEE, 2017, pp. 288–301.
- [31] Y. Ma, Y. Du, L. Du, J. Lin, and Z. Wang, "In-memory computing: The next-generation ai computing paradigm," in *Proceedings of the 2020 on Great Lakes Symposium on VLSI*, 2020, pp. 265–270.
- [32] M. Mao, X. Sun, X. Peng, S. Yu, and C. Chakrabarti, "A versatile reram-based accelerator for convolutional neural networks," in *2018 IEEE International Workshop on Signal Processing Systems (SiPS)*. IEEE, 2018, pp. 211–216.
- [33] S. Mittal, "A survey of reram-based architectures for processing-in-memory and neural networks," *Machine learning and knowledge extraction*, vol. 1, no. 1, pp. 75–114, 2019.
- [34] B. Moons, R. Uytterhoeven, W. Dehaene, and M. Verhelst, "14.5 en-vision: A 0.26-to-10tops/w subword-parallel dynamic-voltage-accuracy-frequency-scalable convolutional neural network processor in 28nm fdsoi," in *2017 IEEE International Solid-State Circuits Conference (ISSCC)*. IEEE, 2017, pp. 246–247.
- [35] B. Murmann, "Adc performance survey 1997-2021 (isscc & vlsi symposium)." <https://web.stanford.edu/~murmann/adcsurvey.html>, 2021.
- [36] T. Norrie, N. Patil, D. H. Yoon, G. Kurian, S. Li, J. Laudon, C. Young, N. Jouppi, and D. Patterson, "The design process for google's training chips: Tpuv2 and tpuv3," *IEEE Micro*, vol. 41, no. 2, pp. 56–63, 2021.
- [37] A. Ofir and G. Ben-Artzi, "Smm-conv: Scalar matrix multiplication with zero packing for accelerated convolution," in *Proceedings of the*

- IEEE/CVF Conference on Computer Vision and Pattern Recognition*, 2022, pp. 3067–3075.
- [38] S. Pal, J. Beaumont, D.-H. Park, A. Amarnath, S. Feng, C. Chakrabarti, H.-S. Kim, D. Blaauw, T. Mudge, and R. Dreslinski, “Outerspace: An outer product based sparse matrix multiplication accelerator,” in *2018 IEEE International Symposium on High Performance Computer Architecture (HPCA)*. IEEE, 2018, pp. 724–736.
- [39] A. Paszke, S. Gross, S. Chintala, G. Chanan, E. Yang, Z. DeVito, Z. Lin, A. Desmaison, L. Antiga, and A. Lerer, “Automatic differentiation in pytorch,” 2017.
- [40] B. Razavi, “Charge steering: A low-power design paradigm,” in *Proceedings of the IEEE 2013 Custom Integrated Circuits Conference*. IEEE, 2013, pp. 1–8.
- [41] B. Reagen, W.-S. Choi, Y. Ko, V. T. Lee, H.-H. S. Lee, G.-Y. Wei, and D. Brooks, “Cheetah: Optimizing and accelerating homomorphic encryption for private inference,” in *2021 IEEE International Symposium on High-Performance Computer Architecture (HPCA)*. IEEE, 2021, pp. 26–39.
- [42] S. Roy, M. Ali, and A. Raghunathan, “Pim-dram: Accelerating machine learning workloads using processing in commodity dram,” *IEEE Journal on Emerging and Selected Topics in Circuits and Systems*, vol. 11, no. 4, pp. 701–710, 2021.
- [43] M. Satyanarayanan, “The emergence of edge computing,” *Computer*, vol. 50, no. 1, pp. 30–39, 2017.
- [44] V. Seshadri, D. Lee, T. Mullins, H. Hassan, A. Boroumand, J. Kim, M. A. Kozuch, O. Mutlu, P. B. Gibbons, and T. C. Mowry, “Ambit: In-memory accelerator for bulk bitwise operations using commodity dram technology,” in *2017 50th Annual IEEE/ACM International Symposium on Microarchitecture (MICRO)*. IEEE, 2017, pp. 273–287.
- [45] W. Shi, J. Cao, Q. Zhang, Y. Li, and L. Xu, “Edge computing: Vision and challenges,” *IEEE internet of things journal*, vol. 3, no. 5, pp. 637–646, 2016.
- [46] H. Shin, J. Sim, D. Lee, and L.-S. Kim, “A pvt-robust customized 4t embedded dram cell array for accelerating binary neural networks,” in *2019 IEEE/ACM International Conference on Computer-Aided Design (ICCAD)*. IEEE, 2019, pp. 1–8.
- [47] H. Shin, D. Kim, E. Park, S. Park, Y. Park, and S. Yoo, “Mcdram: Low latency and energy-efficient matrix computations in dram,” *IEEE Transactions on Computer-Aided Design of Integrated Circuits and Systems*, vol. 37, no. 11, pp. 2613–2622, 2018.
- [48] L. Song, X. Qian, H. Li, and Y. Chen, “Pipelayer: A pipelined rera-based accelerator for deep learning,” in *2017 IEEE International Symposium on High Performance Computer Architecture (HPCA)*. IEEE, 2017, pp. 541–552.
- [49] L. Song, Y. Zhuo, X. Qian, H. Li, and Y. Chen, “Graphr: Accelerating graph processing using rera,” in *2018 IEEE International Symposium on High Performance Computer Architecture (HPCA)*. IEEE, 2018, pp. 531–543.
- [50] P. Srivastava, M. Kang, S. K. Gonugondla, S. Lim, J. Choi, V. Adve, N. S. Kim, and N. Shanbhag, “Promise: An end-to-end design of a programmable mixed-signal accelerator for machine-learning algorithms,” in *2018 ACM/IEEE 45th Annual International Symposium on Computer Architecture (ISCA)*. IEEE, 2018, pp. 43–56.
- [51] H. Valavi, P. J. Ramadge, E. Nestler, and N. Verma, “A 64-tile 2.4-mb in-memory-computing cnn accelerator employing charge-domain compute,” *IEEE Journal of Solid-State Circuits*, vol. 54, no. 6, pp. 1789–1799, 2019.
- [52] A. Vasudevan, A. Anderson, and D. Gregg, “Parallel multi channel convolution using general matrix multiplication,” in *2017 IEEE 28th international conference on application-specific systems, architectures and processors (ASAP)*. IEEE, 2017, pp. 19–24.
- [53] S. Venkataramani, V. Srinivasan, W. Wang, S. Sen, J. Zhang, A. Agrawal, M. Kar, S. Jain, A. Mannari, H. Tran *et al.*, “Rapid: Ai accelerator for ultra-low precision training and inference,” in *2021 ACM/IEEE 48th Annual International Symposium on Computer Architecture (ISCA)*. IEEE, 2021, pp. 153–166.
- [54] O. Villa, D. R. Johnson, M. Oconnor, E. Bolotin, D. Nellans, J. Luitjens, N. Sakharlykh, P. Wang, P. Micikevicius, A. Scudiero *et al.*, “Scaling the power wall: a path to exascale,” in *SC’14: Proceedings of the International Conference for High Performance Computing, Networking, Storage and Analysis*. IEEE, 2014, pp. 830–841.
- [55] J. Wang, X. Wang, C. Eckert, A. Subramaniyan, R. Das, D. Blaauw, and D. Sylvester, “14.2 a compute sram with bit-serial integer/floating-point operations for programmable in-memory vector acceleration,” in *2019 IEEE International Solid-State Circuits Conference-(ISSCC)*. IEEE, 2019, pp. 224–226.
- [56] X. Xie, Z. Liang, P. Gu, A. Basak, L. Deng, L. Liang, X. Hu, and Y. Xie, “Spacea: Sparse matrix vector multiplication on processing-in-memory accelerator,” in *2021 IEEE International Symposium on High-Performance Computer Architecture (HPCA)*. IEEE, 2021, pp. 570–583.
- [57] J. Yang, Y. Kong, Z. Wang, Y. Liu, B. Wang, S. Yin, and L. Shi, “24.4 sandwich-ram: An energy-efficient in-memory bwn architecture with pulse-width modulation,” in *2019 IEEE International Solid-State Circuits Conference-(ISSCC)*. IEEE, 2019, pp. 394–396.
- [58] T. Zhang, K. Chen, C. Xu, G. Sun, T. Wang, and Y. Xie, “Half-dram: A high-bandwidth and low-power dram architecture from the rethinking of fine-grained activation,” in *2014 ACM/IEEE 41st International Symposium on Computer Architecture (ISCA)*. IEEE, 2014, pp. 349–360.